8. R. M. Ruprecht, L. G. O'Brien, L. D. Rossoni, S. Nusinoff-Lehrman, *Nature* **323**, 467–469 (1986).
9. S. D. Young *et al*., *Antimicrob. Agents Chemother.* **39**, 2602–2605 (1995).
10. M. E. Moreno-García, K. M. Sommer, A. D. Bandaranayake, D. J. Rawlings, *Adv. Exp. Med. Biol.* **584**, 89–106 (2006).
11. J. Alcamí *et al*., *EMBO J.* **14**, 1552–1560 (1995).
12. A. Roulston, R. Lin, P. Beauparlant, M. A. Wainberg, J. Hiscott, *Microbiol. Rev.* **59**, 481–505 (1995).
13. W. N. Khan *et al*., *Immunity* **3**, 283–299 (1995).
14. X. D. Li *et al*., *Science* **341**, 1390–1394 (2013).
15. Y. M. Loo, M. Gale Jr., *Immunity* **34**, 680–692 (2011).
16. S. Crawford, S. P. Goff, *J. Virol.* **53**, 899–907 (1985).
17. F. Lori *et al*., *AIDS Res. Hum. Retroviruses* **4**, 393–398 (1988).
18. S. Best, P. Le Tissier, G. Towers, J. P. Stoye, *Nature* **382**, 826–829 (1996).
19. H. Ikeda, F. Laigret, M. A. Martin, R. Repaske, *J. Virol.* **55**, 768–777 (1985).
20. G. B. Beck-Engeser, D. Eilat, M. Wabl, *Retrovirology* **8**, 91-4690-8-91 (2011).
21. D. B. Stetson, J. S. Ko, T. Heidmann, R. Medzhitov, *Cell* **134**, 587–598 (2008).
22. N. Tugnet, P. Rylance, D. Roden, M. Trela, P. Nelson, *Open Rheumatol. J.* **7**, 13–21 (2013).

ACKNOWLEDGMENTS

We thank L. Evans and F. Malik for the generous gift of the 83A25 antibody; P. Jurek for expert assistance in preparing the figures; and the Children's Medical Center Research Institute Flow Cytometry Facility at the University of Texas Southwestern Medical Center for assistance with cell sorting. The data presented in this paper are tabulated in the main paper and in the supplementary materials. This work was supported by generous donations from the Lyda Hill Foundation and the Kent and JoAnn Foster Family Foundation; and by NIH grants P01 AI070167 and U19 AI100627 (to B.B.), R01 AI093967 (to Z.J.C.), and R01 CA157996 (to R.D.).

SUPPLEMENTARY MATERIALS

www.sciencemag.org/content/346/6216/1486/suppl/DC1
Materials and Methods
Supplementary Text
Figs. S1 to S11
Table S1
References (*23*–*32*)

23 June 2014; accepted 6 November 2014
10.1126/science.1257780

REPORTS

ELECTRON TRANSFER

Toward control of electron transfer in donor-acceptor molecules by bond-specific infrared excitation

Milan Delor,[1] Paul A. Scattergood,[1] Igor V. Sazanovich,[1,2] Anthony W. Parker,[2] Gregory M. Greetham,[2] Anthony J. H. M. Meijer,[1] Michael Towrie,[2]* Julia A. Weinstein[1]*

Electron transfer (ET) from donor to acceptor is often mediated by nuclear-electronic (vibronic) interactions in molecular bridges. Using an ultrafast electronic-vibrational-vibrational pulse-sequence, we demonstrate how the outcome of light-induced ET can be radically altered by mode-specific infrared (IR) excitation of vibrations that are coupled to the ET pathway. Picosecond narrow-band IR excitation of high-frequency bridge vibrations in an electronically excited covalent *trans*-acetylide platinum(II) donor-bridge-acceptor system in solution alters both the dynamics and the yields of competing ET pathways, completely switching a charge separation pathway off. These results offer a step toward quantum control of chemical reactivity by IR excitation.

The fundamental process of electron transfer (ET) is central to many light-driven reactions. Light-induced ET in molecules starts by excitation to a so-called Franck-Condon electronic excited state, in which nonzero vibrational levels are usually populated (*1*–*3*). The excess vibrational energy is rapidly lost as the excited state relaxes and nuclear rearrangements begin to occur. ET may occur on time scales commensurate with the depopulation of these "vibrationally hot" states, typically 10^{-14} to 10^{-10} s (*4*), allowing ET to proceed from such nonthermalized states. Previous infrared (IR) spectroscopy studies with vibrational state resolution have shown a significant dependence of ET rates on the vibrational quantum number of the reactant state (*5*). Taken together, these phenomena offer an enticing strategy to influence ET reactions by exciting vibrations coupled with the ET process, thus perturbing nuclear-electronic (vibronic) interactions, which are known to mediate ET in systems ranging from heterogeneous assemblies to complex biological architectures (*6*–*15*). If achieved, this strategy provides a means to alter transition probabilities and ultimately redefine the nature and the yields of products generated in ET processes.

The challenge of directing ET is particularly complex owing to the ultrafast time scales and multicoordinate energy landscape of this class of reactions (*3*). Because the energies of molecular vibrations lie in the IR region, low-energy IR light can be used to target specific vibrations and potentially affect photoreactivity—an approach successfully implemented in gas-phase photochemistry (*16*–*18*). With regard to manipulating photoinduced ET processes, the use of IR light complements existing strategies employing either chemical modifications—for example, of photosynthetic reaction centers (*19*)—or nonlinear laser methods (*20*–*22*) that use ultrashort pulsed laser light in the ultraviolet (UV) or visible spectral regions.

Control of ET processes using IR excitation is underpinned by a strong theoretical framework pertaining to vibronic interactions in the nonadiabatic (weakly electronically coupled) electron tunneling medium. This framework introduces multiple vibronic coupling pathways between electron donor and acceptor, whereby the interference between the electrons propagating through the different pathways directs ET. Theoretical analyses of vibronic tunneling pathways in model molecules by Beratan and co-workers predicted that in inelastic ET reactions, where a tunneling electron may interact and exchange energy with a bridge-localized vibrational mode, IR driving of pathway-specific vibrations can effectively label and select the ET path (*23*–*25*). Such experiments would thus offer the means to control ET reaction outcomes using external IR excitation.

Indeed, vibrational excitation with broadband (~120 cm^{-1}) IR pulses that perturbed the H-bonding network linking donor and acceptor molecules was shown to slow down an intermolecular charge-separation process and decrease its yield by ~1.8% (*26*). These elegant experiments successfully demonstrated the viability of using IR pulses to change the course of an ET reaction.

Our alternative approach to direct ET uses a transform-limited narrowband (~12 cm^{-1}, 1.5 ps) (*27*) IR pulse to achieve mode-specific excitation of intramolecular vibrations directly coupled to ET in a covalently bound donor-bridge-acceptor (DBA) molecular triad. The designed DBA triad **1,** based on a platinum(II)-*trans*-acetylide motif (*28*, *29*), PTZ-CH_2-Ph-C≡C-Pt-C≡C-NAP (*30*), enforces directionality of ET between a powerful electron donor, phenothiazine (PTZ), and an electron acceptor, naphthalene-monoimide (NAP) (Fig. 1A). **1** represents an ideal substrate for IR modulation as the high-frequency C≡C stretching vibrations of the bridge at ~2100 cm^{-1} have previously been identified as the ET reaction coordinate in related Pt(II) acetylides (*31*) and are sufficiently separated in energy and space from the nearest intense IR absorption [~1700 cm^{-1},

[1]Department of Chemistry, University of Sheffield, Sheffield S3 7HF, UK. [2]Central Laser Facility, Research Complex at Harwell, Rutherford Appleton Laboratory, Harwell Science and Innovation Campus, Science and Technology Facilities Council, Chilton, Oxfordshire OX11 0QX, UK.
*Corresponding author. E-mail: mike.towrie@stfc.ac.uk (M.T.), julia.weinstein@sheffield.ac.uk (J.A.W.)

ν(C=O) of the acceptor] to ensure selective vibrational excitation.

The photoinduced processes in **1** have been characterized by a combination of time-resolved infrared (TRIR) and electronic transient absorption spectroscopies (*30*) (see Fig. 1C). The excited-state dynamics are illustrated in Fig. 2, C and D, using TRIR data, collected with a {UV_{pump}, $IR_{broadband\text{-}probe}$} pulse sequence. Absorption of the UV pump partially depopulates the ground electronic state, observed as negative peaks (ground-state bleach), whereas the formation of transient excited states is manifested by positive peaks (excited-state IR absorption) (*32*).

Electronic excitation of **1** with a 400-nm, ~50-fs UV pump initiates ET from the Pt-acetylide center to the NAP acceptor and populates a vibrationally hot charge-transfer manifold, DB^+A^-. This nonthermalized manifold decays over a range of lifetimes from <200 fs to 14 ps, branching over three separate charge transfer pathways (*30*): forward ET from the PTZ donor, forming the full charge-separated state $^3D^+BA^-$ (10% yield, blue arrows in Fig. 2, main IR-band positions 1550, 1605, and 2105 cm^{-1}), which subsequently decays to the ground state with a 1-ns lifetime; population of a long-lived π–π* intraligand triplet state of the NAP acceptor, ^3A (57% yield, 190-μs lifetime, red arrows, main IR-band positions 1590, 1638, and 1950 cm^{-1}); and back ET reforming the ground-state DBA (GS, gray arrows in Fig. 2).

Excited-state branching over multiple ET pathways on the picosecond time scale fulfills an essential requirement to achieve the IR modulation of photoprocesses in **1**. These experiments were performed as follows. Electronic excitation of **1** with a UV pump prepares the vibrationally hot DB^+A^-. A tunable narrowband IR pump is then applied at variable time delays t after the UV pump (Fig. 1B), exciting selected vibrations in DB^+A^-. The product states generated in all reaction pathways are quantified with a broadband IR probe (~400 cm^{-1}) at variable time delays T. Overall, an ultrafast three-pulse {UV_{pump}, $IR_{narrowband\text{-}pump}$, $IR_{broadband\text{-}probe}$} sequence (*33*) is applied to **1** to first initiate ET, then selectively excite vibrations in the bridging unit, and finally probe the changes in the charge transfer dynamics and pathways created by the intermediate IR pump (Fig. 1, B and C). The changes in IR absorption were recorded as $\Delta Abs(IR_{pumpON} - IR_{pumpOFF})$, thereby solely extracting the effect of the IR excitation.

Figure 2, E to H, shows the effect of exciting the ν(C≡C) bridging vibration in DB^+A^- on the photoprocesses in **1**. Clear difference signals from all product states that evolve with time indicate that the IR pump has an effect on both the dynamics and on the relative population of transient states (*34*). When the IR probe arrives at early time delays T after the UV pump (Fig. 2, E and F), the transient IR spectra display pronounced difference signals that indicate a decrease in DB^+A^- (black arrows), and an increase in ^3A (red arrows) and the GS (gray arrows) relative to their population without the IR pump. Thus, IR excitation accelerates charge recombination from the gateway state DB^+A^-. The lack of signals associated with the full charge-separated state $^3D^+BA^-$ at early time delays T suggests no acceleration of forward ET from the donor.

The key observation revealed in Fig. 2, G and H, is that difference signals from the product states caused by the intermediate IR pump persist long after the excitation. Thus, at an IR_{pump}:IR_{probe} delay ($T - t$ in Fig. 1B) of ~98 ps (T = 100 ps, t = 2 ps), the positive signals at 1950, 1638, and 1590 cm^{-1} indicate that IR excitation increases the population of the ^3A state. The negative signals at 2105, 1605, and 1550 cm^{-1} indicate that less $^3D^+BA^-$ is formed. By T = 2.2 ns, most of the $^3D^+BA^-$ (1-ns lifetime) has decayed to the GS. Consequently, the initial decrease in the amount of $^3D^+BA^-$ caused by the IR excitation translates to a lack of ground-state recovery on the nanosecond time scale, resulting in the observed negative GS signals. Thus, the system retains memory of the IR intervention throughout its electronic excited-state lifetime.

The observed IR-modulation effect is mode-specific and is proportional to the IR band intensity of the ν(C≡C) mode in the DB^+A^- state. This conclusion is based on the following: (i) The magnitude of the effect at different IR-excitation frequencies follows the transient IR-absorption

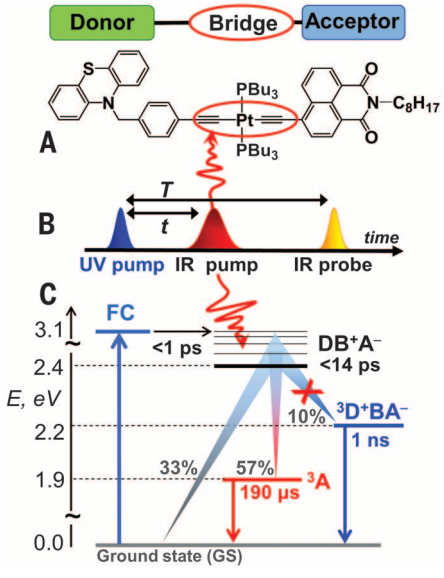

Fig. 1. Schematic of the experiment. (**A**) DBA triad PTZ-CH_2-Ph-C≡C-Pt-C≡C-NAP (**1**). (**B**) Pump-pump-probe pulse sequence used in the IR-modulation experiments. (**C**) The photophysical picture of energetics and dynamics of photoinduced pathways in **1** in CH_2Cl_2 solvent at room temperature. There, the vibrationally hot DB^+A^- manifold branches over three decay pathways to lower electronic states (*30*); "X" denotes the pathway suppressed by intermediate IR excitation. All figures in the paper follow the same color coding.

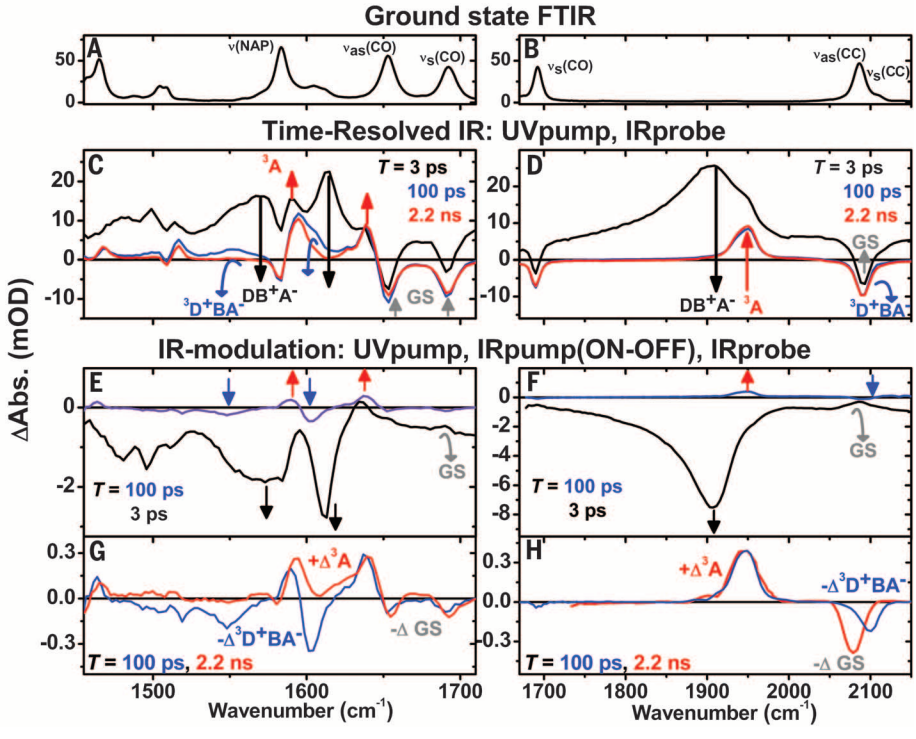

Fig. 2. Excited-state evolution of 1 without and with IR pump in CH_2Cl_2 at room temperature. (**A** and **B**) Ground-state Fourier-transform IR (FTIR) spectra showing vibrational modes before ET is initiated. (**C** and **D**) TRIR spectra after 400-nm excitation at representative UV:IR_{probe} delays T. Corresponding kinetics are in fig. S2. (**E** to **H**) Difference spectra $\Delta Abs(IR_{pumpON} - IR_{pumpOFF})$ at various UV:IR_{probe} delays T with UV:IR_{pump} delay fixed at t = 2 ps, and IR-pump at 1908 cm^{-1} (pulse sequence in Fig. 1B). Arrows indicate formation or decay of a band assigned and color-coded according to the excited states involved; curved arrows represent growth followed by decay of a band.

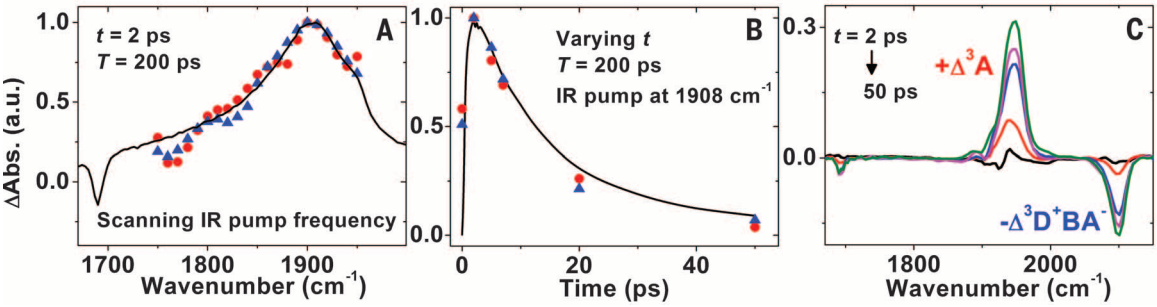

Fig. 3. Action spectrum of IR modulation, scanning IR-pump frequency, and UV: IR_{pump} delay *t*. (**A**) Overlay of the normalized TRIR spectrum of **1** at *T* = 3 ps (—) with the relative magnitudes of population change $\Delta Abs(IR_{pumpON} - IR_{pumpOFF})$ for ^3A (1950 cm^{-1}) (circles) and $^3D^+BA^-$ (negative projection, 2105 cm^{-1}) (triangles) when scanning the IR pump frequency from 1750 to 1950 cm^{-1} in 10 cm^{-1} steps. (**B**) Normalized overlay of a TRIR decay trace at 1908 cm^{-1} (—) with $\Delta Abs(IR_{pumpON} - IR_{pumpOFF})$ for ^3A (circles) and for the negative projection of $^3D^+BA^-$ (triangles) at different UV:IR_{pump} delays *t*. (**C**) Source spectral data for (B).

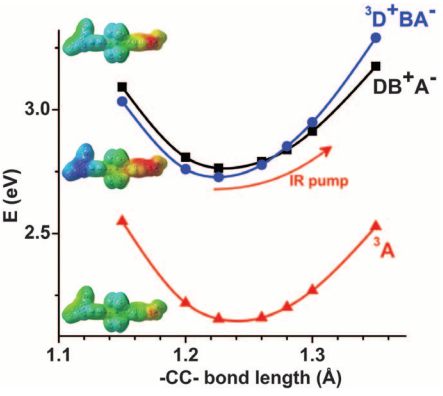

Fig. 4. Calculated potential energy curves and corresponding electrostatic potential maps for 1 in CH_2Cl_2. The curves demonstrate a crossing of states at C≡C bond lengths of the Pt-C≡C-NAP (BA) fragment ~0.04 Å away from equilibrium. Details are given in fig. S8 and table S1. Electrostatic potential maps illustrate the nature of the excited states by the distribution of electron density upon excitation. Charges are color-coded from –0.1 (red) to +0.1 (blue).

profile of the ν(C≡C) vibration in DB^+A^- (Fig. 3A); (ii) the magnitude of the effect also depends on the UV:IR_{pump} delay used. This dependence follows the decay kinetics of DB^+A^- in TRIR experiments (Fig. 3B); (iii) IR excitation of the acceptor-localized ν(C=O) vibration in the same DB^+A^- excited state or of a solvent IR absorption band has no effect (fig. S4), confirming mode specificity and ruling out the influence of local temperature effects.

A quantitative investigation of the effect of the IR excitation revealed that every molecule that absorbs an IR photon has its product states redefined. Without IR excitation, the yield of the full charge-separated state $^3D^+BA^-$ is 10% (*30*). Normalizing to the number of IR photons absorbed by molecules in the gateway DB^+A^- state, we infer that the absolute yield change per IR photon absorbed by the sample is –10 ± 1% for the formation of $^3D^+BA^-$ and +10 ± 1% for ^3A (from 57 to 67%) (*35*). Thus, within experimental error, the data indicate that the pathway to $^3D^+BA^-$ is fully suppressed; forward ET from the donor is completely switched off by selective IR excitation.

In contrast, in a control bridge-acceptor system **2** without the PTZ donor, Ph-C≡C-Pt(PBu_3)$_2$-C≡C-NAP (*30*, *36*), the IR excitation of the ν(C≡C) in the B^+A^- state influences only the rates of ET, but not the product yields (fig. S7). This difference between **1** and **2** suggests that product yield changes in **1** are due to a process specifically affecting the competitive ET pathways between forward electron transfer from the donor and back electron transfer from the acceptor, i.e., between charge separation and recombination across the bridge.

The observed increased rates of ET from higher vibrational levels of a charge-transfer state in both **1** and **2** are consistent with previous studies on the effect of vibrational quantum state on ET dynamics (*5*, *37*, *38*). However, the major changes in product yields and complete suppression of ET in **1** may be better rationalized within the framework of vibronic tunneling pathways (*23*–*25*). The charge transfer state DB^+A^- in **1** can be visualized as a vibronic state from which two ET pathways are available: charge recombination and charge separation. Upon IR excitation of the bridging C≡C oscillator, the latter can exchange energy with a tunneling electron (*24*) and perturb the interferences governing the two ET pathways, modulating ET propensity nonuniformly across the available paths and in this case achieving the observed elimination of the full charge-separated state. From a more general perspective, when ET is mediated by molecular bridges in donor-acceptor systems (*39*, *40*), the bridge structure and its thermal and nuclear motions modulate ET probability (*25*, *41*) by affecting a number of parameters, including electronic and vibronic coupling interactions, which in turn may be affected by IR excitation (*42*).

To explore specifically the effect of the IR excitation of the ν(C≡C) mode in **1** on the relative energies of the excited states involved in ET processes, we performed preliminary time-dependent density functional theory (TD-DFT) calculations for a range of CC distances of the -Pt-CC-NAP fragment (*35*). The CC distances were varied stepwise across the range ± 0.15 Å from the equilibrium distance calculated for the ground-state geometry, and at each distance the energies of multiple excited states were calculated. The results of these calculations for the lowest three excited states (Fig. 4) show a $DB^+A^-/^3D^+BA^-$ state crossover at C≡C bond distances slightly longer than that calculated for the equilibrium geometry. It is therefore feasible that the IR excitation–induced population of a higher vibrational state of the acetylide bridge mode will lead to a transient increase in the average bond length, which could drive the system across this crossover point along the C≡C reaction coordinate, contributing to the experimentally observed suppression of $^3D^+BA^-$ (*43*).

The above results demonstrate a simple and flexible strategy to influence the outcomes of light-induced electron transfer by IR excitation of intramolecular vibrations and suggest the features of molecular design required to achieve such an effect. We show that ultrafast mode-specific IR excitation of bridge vibrations coupled to electron transfer in a *trans*-acetylide Pt(II) donor-bridge-acceptor system in solution can control competing ET channels and ultimately switch between different product states. Direct experimental observation of such effects provides a test bed for theoretical frameworks and can contribute to the understanding of electron transfer processes under nonequilibrium conditions. Overall, directing charge transfer by vibrational excitation may provide hitherto inaccessible insight into chemical mechanisms, in a step toward quantum control of chemical reactivity.

REFERENCES AND NOTES

1. V. Balzani, *Electron Transfer in Chemistry* (Wiley-VCH, Weinheim, Germany, 2001).
2. R. A. Marcus, N. Sutin, *Biochim. Biophys. Acta* **811**, 265–322 (1985).
3. P. F. Barbara, T. J. Meyer, M. A. Ratner, *J. Phys. Chem.* **100**, 13148–13168 (1996).
4. T. Elsaesser, W. Kaiser, *Annu. Rev. Phys. Chem.* **42**, 83–107 (1991).
5. K. G. Spears, X. Wen, R. Zhang, *J. Phys. Chem.* **100**, 10206–10209 (1996).
6. J. Ulstrup, J. Jortner, *J. Chem. Phys.* **63**, 4358–4368 (1975).
7. J. N. Schrauben, K. L. Dillman, W. F. Beck, J. K. McCusker, *Chem. Sci.* **1**, 405–410 (2010).
8. D. Davis, M. C. Toroker, S. Speiser, U. Peskin, *Chem. Phys.* **358**, 45–51 (2009).
9. D. Devault, *Q. Rev. Biophys.* **13**, 387–564 (1980).
10. H. B. Gray, J. R. Winkler, *Annu. Rev. Biochem.* **65**, 537–561 (1996).
11. F. D. Lewis *et al.*, *Proc. Natl. Acad. Sci. U.S.A.* **99**, 12536–12541 (2002).
12. C. Bressler *et al.*, *Science* **323**, 489–492 (2009).
13. C. Shih *et al.*, *Science* **320**, 1760–1762 (2008).
14. J. Repp, P. Liljeroth, G. Meyer, *Nat. Phys.* **6**, 975–979 (2010).
15. A. Halpin *et al.*, *Nat. Chem.* **6**, 196–201 (2014).
16. S. Rosenwaks, *Vibrationally Mediated Photodissociation* (Royal Society of Chemistry, Cambridge, 2009).

17. F. F. Crim, . *J. Phys. Chem.* **100**, 12725–12734 (1996).
18. B. Amstrup, N. E. Henriksen, *J. Chem. Phys.* **97**, 8285–8295 (1992).
19. B. A. Heller, D. Holten, C. Kirmaier, *Science* **269**, 940–945 (1995).
20. M. Shapiro, P. Brumer, *Rep. Prog. Phys.* **66**, 859–942 (2003).
21. V. I. Prokhorenko *et al.*, *Science* **313**, 1257–1261 (2006).
22. G. M. Roberts *et al.*, *Chem. Sci.* **4**, 993–1001 (2013).
23. S. S. Skourtis, D. H. Waldeck, D. N. Beratan, *J. Phys. Chem. B* **108**, 15511–15518 (2004).
24. D. Xiao, S. S. Skourtis, I. V. Rubtsov, D. N. Beratan, *Nano Lett.* **9**, 1818–1823 (2009).
25. H. Carias, D. N. Beratan, S. S. Skourtis, *J. Phys. Chem. B* **115**, 5510–5518 (2011).
26. Z. Lin *et al.*, *J. Am. Chem. Soc.* **131**, 18060–18062 (2009).
27. To influence ET processes by pulsed IR excitation, both IR excitation and ET should occur on time scales shorter than or comparable to that of vibrational relaxation, i.e., typically a few picoseconds, while the minimum ~1.5-ps IR excitation pulse length is required to achieve the sub–12-cm^{-1} pulses necessary for selective vibrational excitation. The chemical system and the experimental setup used in this study fulfill these requirements.
28. C. J. Adams *et al.*, *Inorg. Chem.* **47**, 8242–8257 (2008).
29. J. M. Keller *et al.*, *J. Am. Chem. Soc.* **133**, 11289–11298 (2011).
30. P. A. Scattergood *et al.*, *Dalton Trans.* **43**, 17677–17693 (2014).
31. W. M. Kwok, D. L. Phillips, P. K. Yeung, V. W. Yam, *J. Phys. Chem. A* **101**, 9286–9295 (1997).
32. A broad transient signal appears as a baseline offset that decays with the lifetime of the initially formed DB^+A^- excited-state manifold. This signal is due to a broad electronic absorption profile of the initial charge-transfer state that extends into the mid-IR.
33. P. Hamm, M. Zanni, *Concepts and Methods of 2D Infrared Spectroscopy* (Cambridge Univ. Press, Cambridge, 2011).
34. Pumping the C≡C ν = 0→1 transition with the IR pulse in DB^+A^- is expected to populate ν = 1. A bleach of the ν(0→1) band and a corresponding ν(1→2) transient signal anharmonically shifted to lower energies are expected, as well as similar signals for vibrational modes coupled to the C≡C mode. These signals are characteristic of two-dimensional IR (2DIR) and transient-2DIR spectra (33), which may use similar experimental setups. However, owing to vibronic interactions between different electronic states in **1**, the IR pump gives rise to signals associated with electronic states other than the pumped DB^+A^-.
35. Materials, methods, and additional information are available as supplementary materials on *Science* Online.
36. In diad **2**, the excited state populated as a result of 400-nm excitation is B^+A^-, an equivalent to the DB^+A^- branching state in **1**. However, in **2** no electron donor is present, and therefore no forward electron transfer is possible.
37. K. G. Spears, *J. Phys. Chem.* **99**, 2469–2476 (1995).
38. Y. Huang, C. T. Rettner, D. J. Auerbach, A. M. Wodtke, *Science* **290**, 111–114 (2000).
39. H. M. McConnell, *J. Chem. Phys.* **35**, 508–515 (1961).
40. M. D. Newton, *Chem. Rev.* **91**, 767–792 (1991).
41. I. A. Balabin, J. N. Onuchic, *Science* **290**, 114–117 (2000).
42. D. N. Beratan *et al.*, *Acc. Chem. Res.* **42**, 1669–1678 (2009).
43. Excitation of the high-frequency ν(C≡C) mode will affect other vibrations in its vicinity, which may in turn affect the nature and ordering of the excited states. Presently, exploring this multi-dimensional energy landscape is computationally intractable.

ACKNOWLEDGMENTS

We are grateful to M. Newton (Brookhaven National Laboratory), D. Phillips (Imperial College London), A. Orr-Ewing (Univ. of Bristol), D. Clary (Univ. of Oxford), and G. Worth (Univ. of Birmingham) for comments on the manuscript; to I. Rubtsov and R. Schmehl (Tulane University) for discussions; and to the Engineering and Physical Sciences Research Council, Univ. of Sheffield, and Science and Technology Facilities Council for support.

SUPPLEMENTARY MATERIALS

www.sciencemag.org/content/346/6216/1492/suppl/DC1
Materials and Methods
Figs. S1 to S8
Table S1
References (*44*–*57*)

29 August 2013; accepted 14 November 2014
10.1126/science.1259995

PHOTOCHEMISTRY

One-pot room-temperature conversion of cyclohexane to adipic acid by ozone and UV light

Kuo Chu Hwang* and Arunachalam Sagadevan

Nitric acid oxidation of cyclohexane accounts for ~95% of the worldwide adipic acid production and is also responsible for ~5 to 8% of the annual worldwide anthropogenic emission of the ozone-depleting greenhouse gas nitrous oxide (N_2O). Here we report a N_2O-free process for adipic acid synthesis. Treatment of neat cyclohexane, cyclohexanol, or cyclohexanone with ozone at room temperature and 1 atmosphere of pressure affords adipic acid as a solid precipitate. Addition of acidic water or exposure to ultraviolet (UV) light irradiation (or a combination of both) dramatically enhances the oxidative conversion of cyclohexane to adipic acid.

Adipic acid is a precursor for the synthesis of the nylon-6,6 polymer and, as such, is one of the most important industrial chemical intermediates. More than 3.5 million metric tons of adipic acid were produced in 2013, reflecting a ~5% growth rate per year over the past 5 years (*1*, *2*). Nearly 95% of the worldwide industrial production of adipic acid employed the nitric acid oxidation method (*3*). The first step is air oxidation of cyclohexane under high temperatures (125° to 165°C) and high pressure (8 to 15 atm) to produce KA oil (i.e., a mixture of cyclohexanone and cyclohexanol) with 4 to 11% conversion and ~85% selectivity (*4*, *5*). In the second step, nitric acid is applied as an oxidant: the conversion is ~100%, and the selectivity for adipic acid is 93 to 95% with some other short-chain acids as side products (see Fig. 1A). The process requires the nitric acid–to–KA oil ratio to be maintained at 40:1. Disadvantages of the current industrial process include low overall product yield; corrosion of reaction vessels by nitric acid; emission of the ozone-depleting greenhouse gas N_2O; and high energy consumption. It was estimated that ~0.3 kg of N_2O gas is formed per kilogram of adipic acid produced (*6*, *7*). After energy-consuming recovery and recycling, the amount of N_2O gas released to the atmosphere still accounts for ~5 to 8% of annual anthropogenic N_2O emission worldwide (*3*, *7*, *8*). Many efforts have been devoted to developing more efficient and environmentally friendly processes for industrial production of adipic acid that avoid the emission of N_2O. In 1998, Sato *et al.* reported a process using H_2O_2 as an oxidant to convert cyclohexene to adipic acid in the presence of a Na_2WO_4 catalyst and the phase-transfer reagent $[CH_3(n\text{-}C_8H_{17})_3N]HSO_4$. Although the overall adipic acid yield (93%) is very high (*9*), production of 1 mol of adipic acid requires consumption of 4 to 4.4 mol of H_2O_2. The price of H_2O_2 is ~55% of the price of adipic acid. The requirement of 4 to 4.4 mol of H_2O_2 for production of 1 mol of adipic acid is economically infeasible (*7*). In addition, other negative factors hinder commercialization of this process, including low availability

Department of Chemistry, National Tsing Hua University, Hsinchu, Taiwan, Republic of China.
***Corresponding author. E-mail: kchwang@mx.nthu.edu.tw**

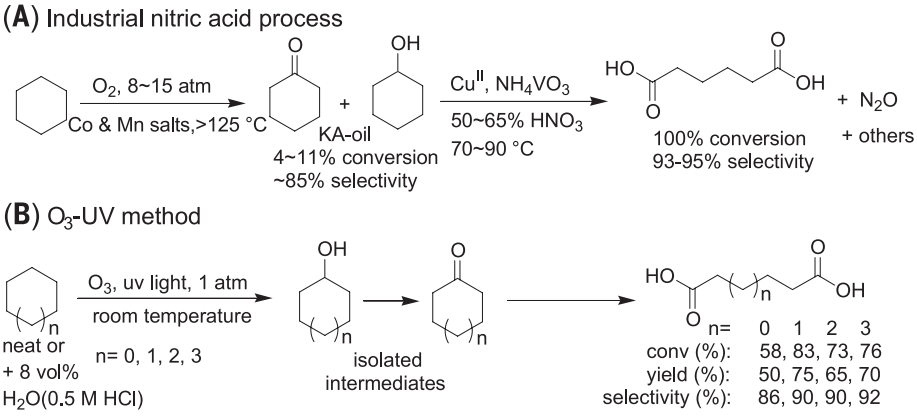

Fig. 1. Comparison of the industrial process and the method presented herein for production of adipic acid. (**A**) Industrial nitric acid process. (**B**) O_3-UV method.

Toward control of electron transfer in donor-acceptor molecules by bond-specific infrared excitation

Milan Delor, Paul A. Scattergood, Igor V. Sazanovich, Anthony W. Parker, Gregory M. Greetham, Anthony J. H. M. Meijer, Michael Towrie and Julia A. Weinstein

Science **346** (6216), 1492-1495.
DOI: 10.1126/science.1259995

Big impact from a well-placed shake

Since the advent of ultrashort laser pulses, chemists have sought to steer reaction trajectories in real time by setting particular molecular vibrations in motion. Using this approach, Delor *et al.* have demonstrated a markedly clear-cut influence on electron transfer probabilities along the axis of a platinum complex. The complex comprised donor and acceptor fragments—which respectively give and take electrons upon ultraviolet excitation—bridged together by triply bonded carbon chains linked to the metal center. By selectively stimulating the carbon triple-bond stretch vibration with an infrared pulse, the authors could induce substantial changes in the observed electron transfer pathways between the fragments.

Science, this issue p. 1492